ACS APPLIED NANO MATERIALS

www.acsanm.org Article

Photoluminescent Si/SiO_2 Core/Shell Quantum Dots Prepared by High-Pressure Water Vapor Annealing for Solar Concentrators, Light-Emitting Devices, and Bioimaging

Kristine Q. Loh, Himashi P. Andaraarachchi, Vivian E. Ferry, and Uwe R. Kortshagen*

Cite This: *ACS Appl. Nano Mater.* 2023, 6, 6444−6453 Read Online

ACCESS | Metrics & More | Article Recommendations | Supporting Information

ABSTRACT: As non-toxic, elementally abundant, and low-cost luminophores, silicon quantum dots (Si QDs) suit a wide variety of applications, from luminescent devices, such as solar concentrators and light-emitting diodes, to bioimaging. Nonthermal plasma-assisted decomposition of silane gas is an efficient, relatively sustainable, and controllable method for synthesizing Si QDs. However, as-synthesized Si QDs have a high defect density and require additional passivation for utilization in these settings. Liquid-based passivation methods, such as thermal hydrosilylation, organically cap Si QDs but cannot prevent oxidation upon exposure to ambient air. Native oxidation effectively passivates the Si QDs and ensures long-term stability in air but typically requires long exposures to ambient conditions. Here, we report the use of high-pressure water vapor annealing (HWA) to quickly obtain Si/SiO_2 core/shell quantum dots with tunable photoluminescence (PL). We first show that the injection of additional hydrogen gas, commonly used in synthesizing organically capped Si QDs, is detrimental to achieving stable silica shells. Then, we demonstrate that varying the applied pressure tunes the PL quantum yield. At higher pressures, the formed silica shells are fully thermally relaxed. Lastly, we report the influence of silica shell thickness, with thicker silica shells leading to environmentally stable quantum yields of >40%. Compared to both thermal hydrosilylation and native oxidation, HWA is a convenient and rapid technique for surface passivation.

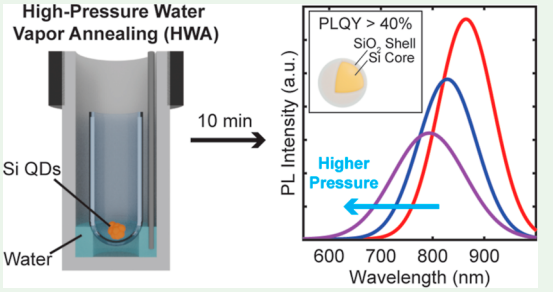

KEYWORDS: *high-pressure water vapor annealing (HWA), silicon quantum dots, silicon oxide, quantum yield, photoluminescence*

INTRODUCTION

Luminescent silicon quantum dots (Si QDs) have garnered increasing interest in a broad variety of applications, including light-emitting diodes (LEDs),[1−4] luminescent solar concentrators,[5−12] and biological imaging.[13,14] Compared to other nanocrystal candidates, Si QDs have advantageous properties including biocompatibility,[14,15] earth abundance,[5] and broad absorption with tunable photoluminescence (PL).[16−18] Si QDs can be synthesized via top-down methods, including anodization of Si wafers into porous Si with subsequent milling[19] and pyrolysis of liquid silicon precursors,[20−22] or bottom-up methods, including nonthermal plasma synthesis.[23−26] This work focuses on nonthermal plasmas as a relatively sustainable synthesis route as this gas-phase method does not use additional solvents or ligands, allows for the synthesis of nanocrystals with narrow size distributions, and requires residence times on the order of milliseconds.[27] Moreover, nanocrystal properties, such as crystallinity and size, can be tuned by adjusting plasma parameters, such as applied power or gas pressure, respectively.[28]

However, as-synthesized Si QDs have high defect densities and low PL quantum yield (PLQY) values, slowing their adoption in optical applications. The typical method for passivation is thermal hydrosilylation, in which organic chains terminate the surface of the Si QDs, leading to PLQY values of up to 60%.[29,30] However, these passivated QDs are still susceptible to oxidative instability even after encapsulation in a polymer composite; after exposure to air, the absolute PLQY drops by over 30% within a few days.[7,31] Furthermore, this method requires the use of additional solvents, partly reducing the sustainability advantages of nonthermal plasma synthesis.

As opposed to direct functionalization with organic ligands, the formation of core/shell nanocrystals offers increased control over the optical and electronic properties of the heterostructure.[32] Type I core/shell quantum dots, in which the band gap of the shell material is wider than that of the core material, confine carriers to the core and enhance the radiative efficiency of the material by increasing the probability of radiative recombination.[33] Native oxidation of plasma-synthesized Si QDs has been shown to effectively protect Si QD cores

Received: March 13, 2023
Accepted: March 24, 2023
Published: April 5, 2023

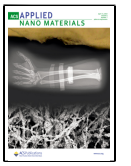

https://doi.org/10.1021/acsanm.3c01130
ACS Appl. Nano Mater. 2023, 6, 6444−6453

through the formation of a silica (SiO_2) shell, leading to moderately high PLQY values above 40%.[34,35] Although this method leads to more stable PLQY values, native oxidation requires at least 30 days of exposure to room air for the silica shell to stabilize and effectively passivate the surface of the Si QD.[35] Therefore, developing methods that accelerate the synthesis of type I core/shell structures with Si QD cores could improve the broad utilization of Si QDs.[31]

High-pressure water vapor annealing (HWA) is another passivation method that has been shown to both reduce defect densities and provide long-term stability in air for various types of silicon, including porous silicon,[36−41] polycrystalline silicon,[42−44] SiO_x/Si films,[45−48] and silicon nanowires.[49] Generally, the termination of defects is due to the formation of thermally relaxed, high-quality Si−O−Si bonds. This method uses relatively low temperatures, in the range of 200−300 °C, and relies on the relationship between temperature and saturation pressure of water to oxidize the silicon materials. In addition to its simplicity, HWA is a scalable method; the distribution of steam throughout the high-pressure chamber ensures uniformity of oxidation.

In 2019, Gelloz et al. reported the first use of HWA for freestanding Si QDs and showed a high absolute PLQY of almost 60% for plasma-synthesized Si QDs made using silicon tetrachloride ($SiCl_4$).[50] These Si/SiO_2 QDs exhibited UV and air stability for over 18 h. However, the tunability of this method to obtain Si QDs of various sizes, and thus various peak PL wavelengths, has not been demonstrated. As one of the key benefits of Si QDs is the quantum-confinement controlled PL, there remains a need for controlling both the absolute PLQY and peak PL wavelengths of Si/SiO_2 QDs while maintaining comparable PLQY values.

Herein, we report the processing of plasma-synthesized Si QDs using only deionized water and relatively low temperatures via HWA. This processing method avoids the use of solvents typically involved in thermal hydrosilylation and provides an improved protective layer for long-term PL stability. In addition to the prevention of continuous oxidation, HWA tunes the PL peak wavelength and PLQY simply by modifying the applied pressure. Furthermore, this method only takes a few hours, including temperature ramping and cooling times, which is orders of magnitude faster than native oxidation.[35] Treating Si QDs with HWA leads to a stable PLQY of >40% in toluene, which is comparable to PLQY values of silane-synthesized Si/SiO_2 QDs previously reported.

EXPERIMENTAL SECTION

Si QD Synthesis. Argon and silane (5% in He) gas flowed into the top of the borosilicate glass plasma reactor tube that widens from 3/8″ OD to 1″ OD, as shown in Figure 1. In the afterglow region, the hydrogen gas flow rate was varied from 0 to 100 sccm. A capacitively coupled plasma was excited by applying radiofrequency power through an impedance matching network to a pair of copper ring electrodes fixed on the outside of the reactor tube. The powered electrode was 4 cm above the point of widening in the reactor tube. Collection of the nanocrystals occurred via inertial impaction[51] as piles of nanocrystals onto a glass slide substrate downstream of the glass tube for all characterization except for Fourier transform infrared (FTIR) spectroscopy. For FTIR spectroscopy, Si QD samples were collected on 0.2 cm × 0.2 cm aluminum-coated Si wafers as a thin film by rastering the wafer below the deposition nozzle.[51] The particles were transferred in argon gas to a nitrogen-purged glovebox for storage and to prevent native oxidation prior to treatment via HWA.

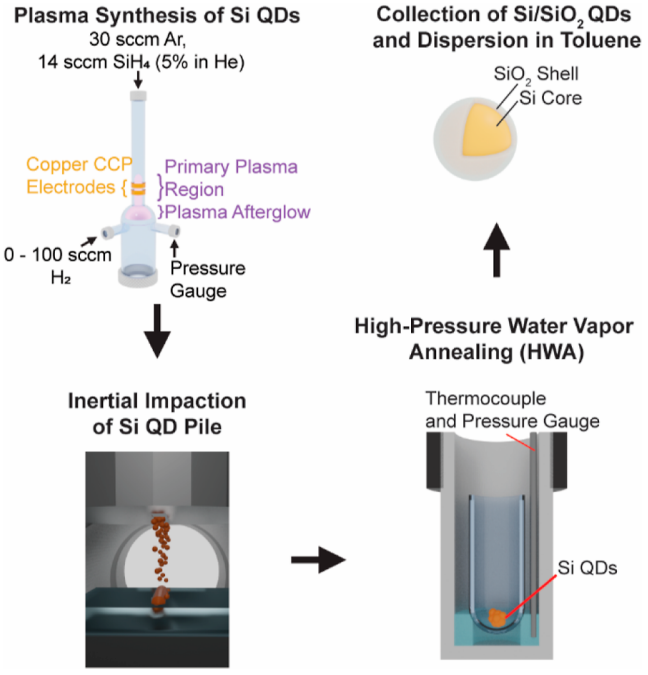

Figure 1. Process schematic.

Oxidation of Si QDs via HWA. HWA was carried out using either a 23 mL acid digestion vessel (model 4749) or a 45 mL high-pressure vessel (model 4700) both purchased from Parr Instrument Company. All HWA experiments were conducted in room air. Initially, for the surface hydride study, the 23 mL vessel was used to contain all samples in one chamber. The Si QDs deposited on glass slides, 0.2 cm × 0.2 cm aluminum-coated Si wafers coated with Si QDs, and deionized water were all loaded into the Teflon liner, such that the water did not contact the Si QDs nor the aluminum side of the Si wafer. The vessel was sealed and placed into a thermal sand bath for heating. Upon the end of the HWA, the vessel was removed from the sand bath and allowed to cool to room temperature for 2 h. The vessel was opened and the dry samples were removed.

For all other studies, the 45 mL vessel was used as this chamber allows for improved pressure control. The Si QDs were removed from the glass slide substrate used for deposition and loaded into a 2 mL glass vial. The vial was placed into a secondary glass container and loaded into the vessel. Deionized water was loaded into the vessel outside of the secondary containment unit to prevent the Si QDs from contacting the water. The applied pressure of the vessel was controlled by controlling the amount of deionized water, similar to the work by Sameshima and Satoh.[45] The vessel was sealed and placed into a thermal sand bath for heating. The 45 mL vessel had both temperature and pressure gauges. Generally, the measured pressure corresponded to the saturation pressure of water at the temperature of the vessel. This relationship is plotted in Figure S1 for the experiments discussed in the main text. The reported pressures and temperatures are experimental values. The vessel was held at the applied pressure for either 10 or 20 min. As holding pressure for 10 min led to improved control and reduced defect densities, as shown in Figure S2, this annealing time was chosen for the studies discussed in the main text. Upon the end of the HWA, the release valve was opened to release the steam from the vessel and end the pressurization. The vessel was then removed from the sand bath and allowed to cool to room temperature for 2 h.

Characterization. The Si/SiO_2 QDs were dispersed in toluene at a concentration of approximately 1 mg/mL for absolute PLQY and time-resolved PL (TRPL) measurements. Dispersion in toluene led to reproducible PLQY measurements over extended periods of time despite the settling of the Si/SiO_2 QDs in the solvent. The lack of complete dispersion in common solvents has been reported previously

https://doi.org/10.1021/acsanm.3c01130
ACS Appl. Nano Mater. 2023, 6, 6444−6453

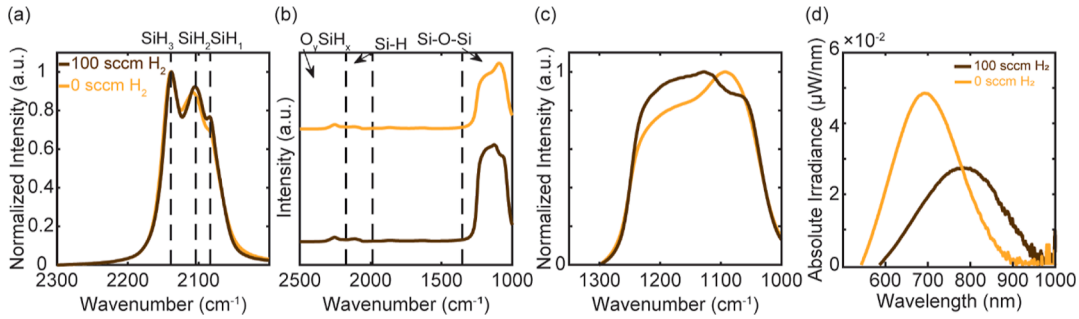

Figure 2. (a) FTIR spectral region between 2000 and 2500 cm^{-1} highlighting the normalized intensities for the SiH_x stretch of as-synthesized Si QDs with hydrogen gas flow rates in the effluent of the plasma ranging from 0 to 100 sccm. Intensities are normalized to the maximum value in this range. (b) FTIR spectral region between 1000 and 2500 cm^{-1} highlighting the O_ySiH_x, SiH_x, and Si−O−Si stretches in oxidized Si QDs. (c) FTIR spectral region between 1000 and 1350 cm^{-1} highlighting the network and cage-structured silica bonds. Intensities are normalized to the maximum value in this range. (d) PL spectra (excitation λ = 395 nm) of oxidized Si QDs dispersed in toluene at a concentration of ∼1 mg/mL.

for Si/SiO_2 QDs.[35] To measure the absolute PLQY, a 2″ general purpose integrating sphere from Labsphere was used, as described by Mangolini et al.,[52] and coupled to an OceanOptics USB-2000 spectrometer. The spectrometer was intensity-calibrated by an OceanOptics HL-3 Plus lamp and wavelength-calibrated by a mercury and an argon calibration source. The integrating sphere also included a baffle placed in front of the detection port. A 395 nm LED inserted into the integrating sphere to excite the sample emitted isotropic radiation via diffuse reflection at the sphere walls. A rhodamine-101 reference was used to confirm both the accuracy and precision of the PLQY absolute irradiance measurement, resulting in a PLQY error of around ±5.5% and peak wavelength measurement error of ±5 nm.[53] To calculate the PLQY, the PL spectra and excitation signal were first converted to photon number. Then, the PL spectra were integrated and divided by the integrated decrease in excitation signal from the LED. These measurements were repeated three times for each sample.

To measure the TRPL decay, a Horiba DeltaFlex time-correlated single-photon counter lifetime fluorometer was used with a Horiba PPD-900 detector. The excitation source was a 405 nm laser with a delay time of 13 μs. The EzTime software paired with the DeltaFlex fluorometer was used to fit the PL decay to a stretched exponential function and to extract both the decay lifetime and the dispersion factor. All fits had a χ-squared value below 1.12, indicating a good fit according to the manufacturer's specifications. For the TRPL measurements, the detector wavelength was set to the peak PL wavelength measured during the computation of the PLQY.

FTIR spectra were taken with a Bruker Alpha FTIR spectrometer with a diffuse reflectance (DRIFTS) accessory in a nitrogen environment. Si/SiO_2 QDs dispersed in toluene were drop-cast onto aluminum-coated Si wafer substrates and allowed to dry for at least 24 h. 24 scans were taken at a 4 cm^{-1} resolution.

To measure relative defect densities, a Bruker continuous wave EleXsys E500 electron paramagnetic resonance (EPR) spectrometer equipped with an X-band (9 GHz) microwave bridge and spherical SHQ resonator was used. Approximately 1 mg of Si/SiO_2 QDs was loaded into NMR grade quartz tubes with a 5 mm diameter and dispersed in 0.1 mL of toluene. The measurements were conducted at ambient temperature in room air.

X-ray diffraction (XRD) was used for structural and size characterization. XRD patterns were taken using a Bruker D8 Discover diffractometer with a Co α (1.79 Å) X-ray source. The data were then mathematically converted to Cu α patterns (1.54 Å) using the MDI JADE software for analysis. Typical collection times were 5 min per frame. As-synthesized Si QDs were analyzed as-deposited on glass slides, and Si/SiO_2 QDs were analyzed by extracting agglomerates of the QDs from the vial after HWA and then attaching them to carbon tape on glass slides. The measurement of oxidized Si QDs to calculate the size of the Si core is possible due to the isolation of characteristic crystalline Si peaks in the spectra. HWA-treated Si QDs comprise a crystalline Si core and an amorphous SiO_2 shell. Figure S3 shows the XRD spectrum of amorphous SiO_2 QDs obtained by treating Si QDs at much higher pressures. The crystallinity of the Si QDs was confirmed according to the crystalline Si structure ($cFd\bar{3}m$, PDF 98-001-9306). Crystallite sizes were estimated using Scherrer fits of the (220) peak according to the following Scherrer formula that has been adapted for nearly spherical nanocrystals: $d = 4K\lambda//(3w\cos\theta)$, where K is the shape factor, λ is the wavelength of the X-ray source, w is the FWHM of the (220) peak, and θ is the peak position.[54,55] Assuming nearly spherical particles, the shape factor was 0.89.

X-ray photoelectron spectroscopy (XPS) was performed for additional surface characterization and a PHI VersaProbe III was used with a monochromatic Al Kα anode X-ray source (photon energy = 1486.6 eV) and a hemispherical analyzer. The carbon 1s peak at 284.6 eV was used as a reference. Survey and high-resolution scans were acquired with 280 and 55 eV pass energies, respectively. The PHI SmartSoft XPS package was used to acquire the data and PHI Multipack v9.0 analyzed it. Dry samples similar to those used for XRD characterization were used.

Transmission electron microscopy (TEM) to perform structural characterization was conducted using a Thermo Scientific FEI Talos F200x transmission electroscope operating at an accelerating voltage of 200 kV. TEM samples post-oxidation were collected on thin C-coated Cu grids by drop-casting particles dispersed in toluene. Selective area diffraction patterns and lattice parameters were analyzed using ImageJ.

RESULTS AND DISCUSSION

Influence of Effluent Hydrogen Gas Injection Prior to Oxidation. Hydrogen-terminated Si QDs were synthesized according to a previously published method.[56] Anthony et al. showed that hydrogen gas injection in the afterglow region of the plasma is critical for high PLQY values of thermally hydrosilylated Si QDs because hydrogen terminates surface Si sites that are not terminated by an attached organic ligand. However, initial HWA trials conducted with hydrogen gas injection resulted in PLQY values of only a few percent regardless of annealing time or temperature. To illustrate the impact of hydrogen gas injection during synthesis on the luminescence of HWA-treated Si QDs, we studied Si QDs synthesized using various hydrogen gas flow rates with FTIR both prior to and post HWA treatment. Figure 2 shows FTIR and PL data for as-synthesized and oxidized Si QDs made using 0 and 100 sccm of hydrogen gas. Figure S4 also provides additional data for 77 and 87 sccm of hydrogen. Figure 2a demonstrates that prior to HWA, regardless of the hydrogen gas flow rate, the SiH_3 peak dominates relative to the SiH_2 and SiH peaks, indicating a more complete coverage of Si QD surface states with hydrogen atoms. However, after oxidation,

https://doi.org/10.1021/acsanm.3c01130
ACS Appl. Nano Mater. 2023, 6, 6444−6453

the Si/SiO_2 QDs have varied silica shell structures as shown in Figure 2b,c and subsequent PL intensities as shown in Figure 2d. The FTIR peaks in the range of 2000−2500 cm^{-1} indicate the formation of the silica shell in the presence of moisture as the SiH_x peaks decrease while the O_xSiH_y peaks increase in intensity. The peaks in the range of 1000−1300 cm^{-1} of the FTIR spectra indicate the differences in the silica shell bond angles across the different synthesis conditions; no hydrogen injection in the afterglow region of the plasma leads to the formation of the more stable network structure of silica as indicated by a silica peak around 1070 cm^{-1}.[57] These trends in the Si−O−Si peak agree with previous findings by Pereira et al.[58] as Si/SiO_2 QDs with a lower defect density had a similar dominance of the network-structure peak at ∼1070 cm^{-1} while Si/SiO_2 QDs with higher defect densities had a higher frequency shoulder at a higher intensity. In contrast, flowing 100 sccm of hydrogen gas in the effluent of the plasma results in the less-stable cage-structured silica, as indicated by the more dominant shoulder in the 1100−1500 cm^{-1} region.

While size effects may confound the variances in the PL intensity as Si QDs have the highest PL intensity when the peak PL wavelength is around 850 nm,[59] the higher PL intensity and formation of the thermally relaxed network-structured silica shell indicate that synthesizing Si QDs without hydrogen injection in the afterglow leads to higher quality Si/SiO_2 QDs when processed via HWA. This is distinctly different from organically capped Si QDs, which require hydrogen injection during synthesis to reach high PLQY values.[34] Furthermore, these findings indicate the difference between studying natively oxidized Si QDs and HWA-treated Si QDs as other studies have indicated that natively oxidized Si QDs synthesized with hydrogen gas have reduced defect densities relative to those synthesized without hydrogen gas.[26,35,58,60] For example, Pereira et al. found that Si QDs synthesized with hydrogen gas in their work had a more thermally relaxed, network-structured silica shell, similar to the HWA-treated Si QDs synthesized without hydrogen gas in this work.[58] In contrast, Si QDs synthesized without hydrogen gas had a more cage-structured silica shell after native oxidation, similar to the HWA-treated Si QDs synthesized here with hydrogen gas. This comparison points to the need for scrutiny in comparing HWA-treated Si QDs to natively oxidized Si QDs; however, this investigation is outside the scope of this work. For the following studies, we focus on Si QDs that were synthesized without additional hydrogen gas injection as those yielded the best PL properties with HWA posttreatment.

Influence of Applied Pressure. We next examine the influence of pressure on the PLQY and PL spectra of HWA-treated Si QDs. Figure 3a shows the measured PL intensities of Si QDs oxidized from 7.5 to 17 bar. Increasing the pressure of the vessel generally blue-shifts the PL of the Si/SiO_2 QDs, and the intensities decrease as the peak PL wavelength strays from 850 nm, where generally the optimal PLQY of Si QDs is observed.[59] Similarly, Figure 3b shows that both the PLQY and the peak PL wavelength decrease with increasing pressure. In accordance with quantum confinement, higher pressures lead to smaller Si cores, which exhibit blue-shifted PL. This correlation has also been corroborated via XRD as shown in Figure S5 since Si/SiO_2 QDs with blue-shifted PL spectra have smaller measured Si cores, as calculated using Scherrer fits. In addition, these values were measured after the HWA-oxidized samples were exposed to room air for at least 24 h. When treated at lower pressures, the absolute PLQY decreases by

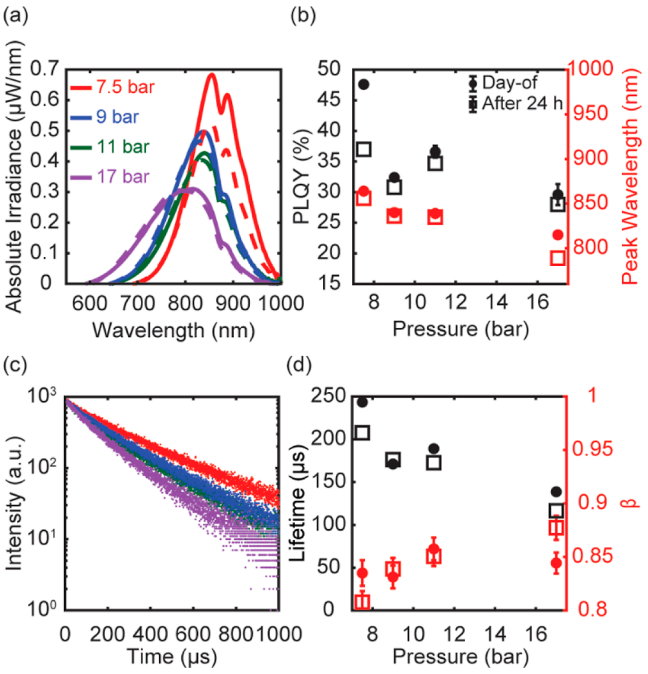

Figure 3. (a) PL spectra of oxidized QDs treated at different pressures taken on the day of oxidation (solid lines) and at least 24 h after HWA (dashed lines). The feature at 880 nm is attributed to an absorption feature of toluene. (b) PLQY and peak PL wavelength as a function of applied pressure captured on the day of oxidation (solid circles) and at least 24 h after HWA (open squares). (c) TRPL decays of oxidized QDs detected at the samples' respective peak PL wavelength. (d) Fluorescence lifetimes and dispersion factors (β) of oxidized QDs as a function of pressure captured on the day of oxidation (solid circles) and at least 24 h after HWA (open squares). Error bars smaller than symbols are not shown.

over 10% while the peak PL wavelength does not change significantly. However, when treated at higher pressures, the PLQY does not decrease as drastically. Notably, the decreases in PLQY for HWA-oxidized Si QDs are not as significant as those for thermally hydrosilylated Si QDs, which exhibit a decrease in PLQY by over 30% over a few days of air exposure even when encapsulated by a polymer.[7]

Studying the influence of pressure on the TRPL decay also provides insights into the factors that drive the trends in the PLQY. Figure 3c shows that the TRPL decay curve follows a stretched exponential behavior that is typical for Si QDs: $I(t) = I_0 \exp[-(t/\tau)^{\beta}]$, where I_0 is the PL intensity at time $t = 0$ μs, τ is the fluorescence lifetime, and β is the dispersion factor.[61] The PLQY is also described by PLQY = $\tau\Gamma_r$, where Γ_r is the radiative recombination rate. The fluorescence lifetimes and dispersion factors shown in Figure 3d were extracted from the TRPL decay curves and explain the trends in the PLQY as well. With increasing pressure, the fluorescence lifetimes decrease. Fluorescence lifetimes on the order of hundreds of microseconds are characteristic of core-related emission, or "slow" band PL, for Si QDs in the quantum confinement regime.[61] These long lifetime values also indicate that the PL does not originate from defects in the oxide as no blue PL is present; the maintenance of the crystalline Si core after treatment via HWA leads to these long lifetimes. Similar to the trend in the PLQY values, after at least 24 h, the lifetimes decrease most significantly when the Si QDs are treated at lower pressures. Conversely, with increasing pressure, the

https://doi.org/10.1021/acsanm.3c01130
ACS Appl. Nano Mater. 2023, 6, 6444−6453

dispersion factors increase. Moreover, the dispersion factors increase over time as shown in the 17 bar case. This may point to the ensemble of QDs stabilizing over time as dispersion factors closer to 1.0 (single-exponential decay) indicate a closer proximity of the system to the ideal, isolated QD system.[59] These results show that the PL of Si/SiO_2 QDs can be tuned simply by tuning the pressure during HWA treatment, which can be considered a design parameter to tailor Si QD luminescence properties to specific applications.

We then used FTIR measurements to study the surface structure of the Si/SiO_2 QDs and gain additional insight into the trend in PLQY values with varying pressure. Figure 4

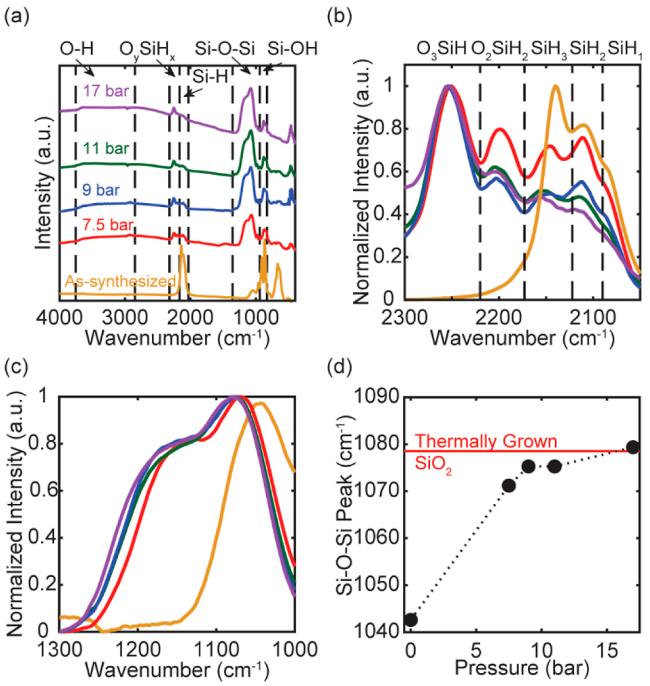

Figure 4. (a) FTIR spectra of as-synthesized (yellow) and oxidized Si QDs treated at 7.5−17 bar. (b) FTIR spectral region between 2000 and 2300 cm^{-1} highlighting Si−H stretching for silicon back-bonded to oxygen atoms, O_ySiH_x and SiH vibrations, SiH_x. Intensities are normalized to the maximum value in this range. (c) FTIR spectral region between 1000 and 1300 cm^{-1} highlighting Si−O−Si stretching vibrations. Intensities are normalized to the maximum value in this range. (d) Peak wavenumbers of the Si−O−Si feature as a function of pressure. The point at 0 bar refers to as-synthesized Si QDs. The dotted line is included to guide the eye.

shows the FTIR spectra of the as-synthesized Si QDs as well as the Si QDs oxidized at pressures ranging from 7.5 to 17 bar. Figure 4a shows the FTIR spectra of these samples in the 400−4000 cm^{-1} range, and multiple peaks are observed that indicate the formation of a silica shell for the oxidized QDs, including −OH, Si−O−Si, and Si−OH peaks. Weeks et al. reported that the presence of Si−OH bonds was critical for efficient light emission from Si QDs treated with low-pressure steam.[62] Their work on low temperature oxidation of Si QDs reported that the PL intensity of Si QDs could only be enhanced in the presence of water vapor, not O_2 alone. From 2000−2150 and 2150−2300 cm^{-1}, the peaks in Figure 4b correspond to various stretching modes of SiH_x bonds and O_xSiH_y surface bonds, respectively.[57] Prior to oxidation, the SiH_3 feature is the most significant. After oxidation, all samples exhibit a decrease in the intensity of the SiH_3 vibration and the SiH_2 vibration becomes the most significant of the three SiH_x vibrations in this range. As HWA causes initially non-luminescent QDs to exhibit PL, these features align with the conclusion by Shu et al. that for plasma-synthesized nanocrystals, higher PLQY values are observed when the SiH_3 features in the FTIR spectra are less dominant.[63] In that study, the increase in PLQY was associated with the removal of physisorbed SiH_3 groups that led to nonradiative recombination; the SiH_2 vibration had the highest intensity for high PLQY Si QDs. The features we observe in the 2150−2300 cm^{-1} range correspond to Si−H stretching for silicon back-bonded to oxygen atoms, with O_2SiH_2 at 2200 cm^{-1} and O_3SiH at 2249 cm^{-1}.[64] The emergence of these peaks after HWA indicates the development of a silica shell through the presence of water vapor[65] and, in conjunction with the presence of the Si−O−Si peak, suggests the full formation of a silica shell while maintaining an intact Si core.[35,58,66,67]

Figure 4c shows the peaks in the 1000−1300 cm^{-1} range that correspond to Si−O−Si bonds. The key parameter in this figure is the peak wavenumber as this gives an indication of the stoichiometry of the silica shell. Prior to HWA, the as-synthesized Si QDs not exposed to air exhibit a small peak at 1045 cm^{-1} that may be due to residual moisture or contamination from etching of the glass tube wall.[26] Nevertheless, this peak indicates the formation of near-stoichiometric silica ($SiO_{1.7-1.8}$) that also corresponds to a higher defect density compared to stoichiometric silica.[57] Figure 4d summarizes the peak wavenumber for the Si−O−Si bond both prior to and post-HWA. Upon oxidation via HWA, the peak wavenumber increases to above 1070 cm^{-1}, corresponding to the formation of stoichiometric silica ($SiO_{2.0}$). As the applied pressure increases, the peak wavenumber increases as well. At the highest applied pressure, 17 bar, the peak wavenumber surpasses that for thermally grown silica, 1078.5 cm^{-1}, with Si−O−Si bonds in their fully thermally relaxed state.[68]

To further confirm the chemical state on the surface of the Si/SiO_2 QDs, we performed additional surface characterization through XPS, as shown in Figure S6. The sample chosen for characterization was that treated at 11 bar. The deconvoluted Si 2p spectrum exhibits three peaks. The peak at 103.5 eV corresponds to Si^{4+}, suggesting that the surface mainly comprises fully oxidized Si (SiO_2). The peak at 102.5 eV corresponds to Si^{3+}, which indicates the presence of silicon suboxides in the surface layer. The Si^0 peak at 99.5 eV indicates that the crystalline Si core remains intact after oxidation and has the lowest contribution due to the nature of the XPS surface characterization. The peaks in the O 1s spectrum indicate the presence of both pristine SiO_2, as indicated by the largest contributing peak at 532.8 eV, and a suboxide, as indicated by the peak at 531.3 eV. Both spectra confirm the presence of Si−O bonds due to the silica shell and the maintenance of the metallic Si core after oxidation.

Influence of Silica Shell Thickness. While HWA tunes the optical properties of Si/SiO_2 QDs, it is unclear whether the thickness of the silica shell or the size of the Si core controls the PLQY. For Si QDs, the PL intensity is highest when the Si core is close to the size of the Bohr exciton radius.[59] However, the additional factor of the silica shell thickness confounds the trends in PLQY shown in Figure 3. Selvan et al. reported a parabolic relationship between silica shell thickness and PLQY, suggesting that there is an optimal silica shell thickness for high PLQY values.[69] Therefore, the variables of silica shell thickness and Si core size proximity to the Bohr exciton radius require

https://doi.org/10.1021/acsanm.3c01130
ACS Appl. Nano Mater. 2023, 6, 6444−6453

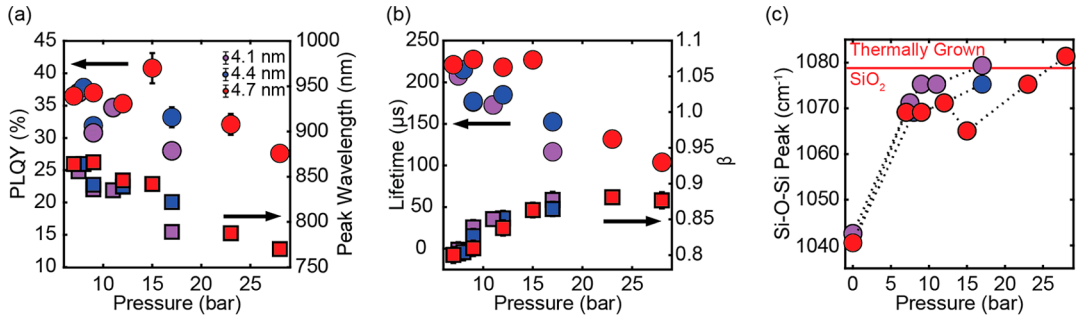

Figure 5. (a) PLQY and peak wavelength of oxidized Si QDs as a function of pressure captured at least 24 h after HWA for 4.1, 4.4, and 4.7 nm as-synthesized Si QDs. (b) Fluorescence lifetimes and dispersion factors of oxidized Si QDs as a function of pressure captured at least 24 h after HWA at the samples' respective peak PL wavelength. (c) Si−O−Si peak wavenumbers as a function of pressure of oxidized Si QDs. Error bars smaller than symbols are not shown.

additional investigation and separation to better understand the main factors that drive the PLQY of Si/SiO_2 QDs. As oxidation via HWA reduces the size of the Si core to form the SiO_2 shell, larger Si QDs were synthesized following the synthesis parameters in Table S1. By decreasing the size of the deposition orifice, the upstream pressure of the plasma was increased, which increased the residence time needed to develop larger nanocrystals. The sizes of the as-synthesized QDs were characterized using XRD shown in Figure S7. By synthesizing larger QDs, samples with the same Si core size but varying silica shell thicknesses can be directly compared.

We first show the versatility of HWA for oxidizing Si QDs of different sizes. Figure 5a shows the PLQY values of 4.1, 4.4, and 4.7 nm Si QDs oxidized at various pressures. The data shown in Figure 5 for 4.1 nm are the same as those shown in Figure 3 but replotted here for direct comparison with larger Si QDs. Across all sizes tested, the PLQY generally decreases with increasing pressure as the peak PL wavelength deviates from 850 nm. The exception to this trend is the 4.7 nm QD sample treated at 15 bar, which had the highest PLQY value of 41%. Previously, Gelloz et al. studied the influence of pressure on HWA-treated porous Si samples and found that optimizing the pressure significantly enhanced the external quantum efficiency.[37] In that study, applied pressures lower than the optimum resulted in lower PL intensities, while applied pressures higher than the optimum resulted in over-oxidation and reduced PL intensities as well. Similarly, the optimized applied pressure of 15 bar resulted in the highest PL intensity for Si/SiO_2 QDs. Smaller QDs treated at lower pressures have the same final peak PL wavelength as 4.7 nm QDs treated at higher pressures; larger QDs need higher pressures to arrive at the same Si core size. The extracted fluorescence lifetimes and dispersion factors for the TRPL decays from each sample detected at each sample's respective peak PL wavelength are plotted in Figure 5b. For 4.1 and 4.4 nm as-synthesized Si QDs, the lifetime generally decreases with increasing pressure. Interestingly, for 4.7 nm Si QDs, the lifetime values for the samples treated at 7−15 bar have similar lifetime values of around 230 μs. The variation in the PLQY despite the similar lifetime values may be due to the conversion of "dark" or "blinking" QDs to "bright" QDs. This phenomenon has been reported before by both Li et al. and Sangghaleh et al.;[30,70] processing conditions, such as in-flight heating or dispersion in an appropriate polymer matrix, convert the "dark", non-radiative QDs in the QD ensemble to those with a high internal quantum efficiency. As the dispersion factor for the samples treated at 7−15 bar increases with increasing pressure but the lifetimes stay the same, it can be inferred that in this pressure range, higher pressure improves the quantum efficiency of the QD ensemble. To further understand the improvements in the formation of the silica shell that may have led to the higher PLQY values, Figure 5c displays the peak wavenumbers of the Si−O−Si features in the FTIR spectra for each sample. As the applied pressure increases, the peak wavenumber generally increases as well, even surpassing that of thermally grown SiO_2 at high enough pressures. This trend aligns with that reported by Sameshima et al., which used HWA for treating SiO_2 films.[45] With increasing amounts of water used to increase the applied pressure, the peak wavenumber increased, suggesting that higher pressures improve silica network uniformity.

Although the data plotted in Figure 5 demonstrate the tunability of the PLQY with pressure, it is still unclear as to whether silica shell thickness or the Si core size dictates the PLQY values presented. Figure 6 replots the data in Figure 5 with respect to the peak PL wavelength instead, as this

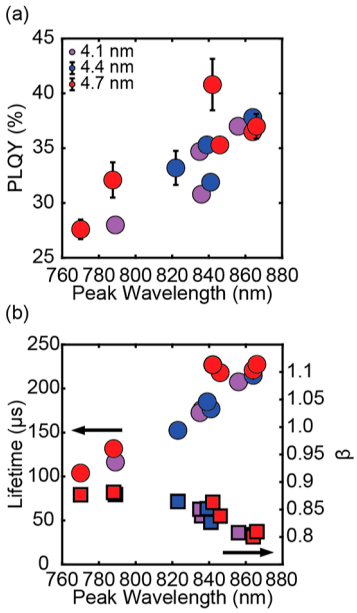

Figure 6. (a) PLQY as a function of peak PL wavelength captured at least 24 h after HWA. (b) Fluorescence lifetimes and dispersion factors as a function of peak PL wavelength captured at least 24 h after HWA at the samples' respective peak PL wavelengths. Error bars smaller than symbols are not shown.

https://doi.org/10.1021/acsanm.3c01130
ACS Appl. Nano Mater. 2023, 6, 6444−6453

parameter is correlated with the Si core size per the quantum confinement effect.[61] Figure 6a clearly suggests that the thicker the silica shell, as indicated by the larger as-produced Si QD size, the higher the PLQY. At a peak PL wavelength of around 840−850 nm, closest to the size of the Si Bohr exciton radius,[59] the 4.7 nm Si QDs treated at 15 bar had the highest PLQY. Figure S8 also shows that the absolute PLQY decreases to around 35% after the sample had been stored in air for over 3 months.

This trend continued for other samples with more blue-shifted PL, as samples with a PL maximum of around 790 nm also showed that thicker silica shells led to higher PLQY values. While the as-synthesized 4.7 nm Si QD samples with peak PL wavelengths longer than 850 nm seem to not follow this trend in Figure 6a, these data points emphasize the importance of applied pressure on the resulting PLQY. These samples were oxidized at pressures lower than 15 bar and thus had thinner silica shells that led to lower PLQY values. Figure 6b shows that, consistent with the PLQY measurements, the lifetimes increase with increasing peak PL wavelength and the lifetimes are the longest for the oxidized 4.7 nm Si QDs. The dispersion factors are also the highest for oxidized 4.7 nm Si QDs but are all within a high range of 0.8 to 0.9. While the PLQY values may be lower at shorter wavelengths, the high dispersion factors indicate the high quality of the samples.

Finally, to confirm the core/shell structure of the Si/SiO_2 QDs, we collected TEM images of the champion sample with the highest PLQY, as shown in Figure S9. The images of the oxidized sample were collected after the sample had been stored in air for over 6 months, suggesting that the silica shell persists over time. The TEM images of this champion sample show a crystalline core surrounded by an amorphous shell post-oxidation, confirming the maintenance of the crystalline Si core after HWA treatment as well. The Si/SiO_2 QDs in this ensemble had a core of around 4.1 nm with a shell of around 1 nm thickness, aligning with the calculated Scherrer size. The Si core also exhibits lattice fringes that can be indexed to the Si (111) plane. The calculation of the 0.32 nm *d*-spacing indicates the absence of strain in this material as the calculated lattice constant agrees with that expected for the Si (111) plane. With these images, we can assume that all Si/SiO_2 QDs oxidized via HWA presented in this work also contain a core/shell structure and have high PLQY values due to the protective silica shell.

CONCLUSIONS

We demonstrate here that HWA is a versatile method for passivating Si QDs synthesized via nonthermal plasma-assisted decomposition of silane gas. By simply tuning the applied pressure, we tuned the thickness and quality of the silica shell, which strongly influence the PLQY, peak PL wavelength, and fluorescence lifetime. The PL intensities of the Si/SiO_2 QDs were higher when the QDs were not synthesized with hydrogen gas due to the differences in the bond angles in the silica network. Si/SiO_2 QDs with a high, stable PLQY exceeding 40% were obtained from oxidizing 4.7 nm Si QDs at 15 bar. This value is comparable to those achieved via native oxidation[35] and are higher than those reported for thermally hydrosilylated Si QDs exposed to air.[7,9] While this value is not record-breaking, the minimal time required to successfully passivate the Si QDs and the tunability of the system may improve the utilization of this material in practical applications, including optoelectronic devices and bioimaging technologies.

Compared to other passivation methods for Si QDs, HWA offers tunability and comparable PLQY values without the need for extended periods of time for native oxidation[35] or the need for solvents and additional chemical precursors for hydrosilylation.[52] At relatively low temperatures and pressures, HWA successfully passivates defects at the Si QD surface and results in a relaxed, stable oxide shell that allows for sufficient environmental protection for over 3 months.

ASSOCIATED CONTENT

Supporting Information

The Supporting Information is available free of charge at https://pubs.acs.org/doi/10.1021/acsanm.3c01130.

Experimental details on the HWA parameters, characterization of Si/SiO_2 QDs treated for 10 and 20 min via HWA, XRD spectra of over-oxidized, amorphous SiO_2 QDs and as-synthesized Si QDs, FTIR and PL characterization of oxidized Si QDs made using 0−100 sccm H_2, calculated Si core sizes from Scherrer fits, high-resolution XPS spectra, synthesis conditions for the Si QDs, PL spectra with associated PLQY values for the champion sample after 105 days, and HRTEM images of the champion sample (PDF)

AUTHOR INFORMATION

Corresponding Author

Uwe R. Kortshagen − *Department of Mechanical Engineering, University of Minnesota, Minneapolis, Minnesota 55455, United States;* orcid.org/0000-0001-5944-3656; Email: kortshagen@umn.edu

Authors

Kristine Q. Loh − *Department of Chemical Engineering and Materials Science, University of Minnesota, Minneapolis, Minnesota 55455, United States;* orcid.org/0000-0001-5205-157X

Himashi P. Andaraarachchi − *Department of Mechanical Engineering, University of Minnesota, Minneapolis, Minnesota 55455, United States;* orcid.org/0000-0001-9736-1088

Vivian E. Ferry − *Department of Chemical Engineering and Materials Science, University of Minnesota, Minneapolis, Minnesota 55455, United States;* orcid.org/0000-0002-9676-6056

Complete contact information is available at: https://pubs.acs.org/10.1021/acsanm.3c01130

Author Contributions

All authors participated in the conception and design of the experiments. K.Q.L. performed all experiments and analyzed the data, except for the XPS spectra in Figure S6 and the HRTEM images in Figure S9. H.P.A. conducted the XPS and TEM characterization and related data analysis. All authors discussed the data and contributed to the analysis. K.Q.L. drafted the manuscript. All authors read and edited the manuscript and gave approval to the final version.

Notes

The authors declare no competing financial interest.

ACKNOWLEDGMENTS

The University of Minnesota—Twin Cities resides on Dakota land that was acquired through the Land Cession Treaties of

1837 and 1851. We acknowledge the legacies of violence, displacement, migration, and settlement that comes with our use of this land. The authors acknowledge partial support from the Minnesota Environment and Natural Resources Trust Fund (M.L. 2018, Chp. 214, Art. 4, Sec. 02, Subd. 07a). K.Q.L. was partially supported by the National Science Foundation Graduate Research Fellowship under grant no. 2237827 and received support from the University of Minnesota under the Ronald L. and Janet A. Christenson Chair in Renewable Energy. Parts of this work were carried out in the Characterization Facility, University of Minnesota, which receives partial support from the NSF through the MRSEC (award number DMR-2011401) and the NNCI (award number ECCS-2025124) programs. The EPR experiments reported in this paper were performed at the Biophysical Technology Center, University of Minnesota Department of Biochemistry, Molecular Biology, and Biophysics.

REFERENCES

(1) Cheng, K.-Y.; Anthony, R.; Kortshagen, U. R.; Holmes, R. J. High-Efficiency Silicon Nanocrystal Light-Emitting Devices. *Nano Lett.* **2011**, *11*, 1952−1956.
(2) Zhang, Y.-C.; Yu, Z.-Y.; Xue, X.-Y.; Wang, F.-L.; Li, S.; Dai, X.-Y.; Wu, L.; Zhang, S.-Y.; Wang, S.-Y.; Lu, M. High Brightness Silicon Nanocrystal White Light-Emitting Diode with Luminance of 2060 Cd/m^2. *Opt. Express* **2021**, *29*, 34126−34134.
(3) Xu, Y.; Terada, S.; Xin, Y.; Ueda, H.; Saitow, K. i. Ligand Effects on Photoluminescence and Electroluminescence of Silicon Quantum Dots for Light-Emitting Diodes. *ACS Appl. Nano Mater.* **2022**, *5*, 7787−7797.
(4) Yamada, H.; Saitoh, N.; Ghosh, B.; Masuda, Y.; Yoshizawa, N.; Shirahata, N. Improved Brightness and Color Tunability of Solution-Processed Silicon Quantum Dot Light-Emitting Diodes. *J. Phys. Chem. C* **2020**, *124*, 23333−23342.
(5) Meinardi, F.; Ehrenberg, S.; Dhamo, L.; Carulli, F.; Mauri, M.; Bruni, F.; Simonutti, R.; Kortshagen, U.; Brovelli, S. Highly Efficient Luminescent Solar Concentrators Based on Earth-Abundant Indirect-Bandgap Silicon Quantum Dots. *Nat. Photonics* **2017**, *11*, 177−185.
(6) Huang, J.; Zhou, J.; Haraldsson, T.; Clemments, A.; Fujii, M.; Sugimoto, H.; Xu, B.; Sychugov, I. Triplex Glass Laminates with Silicon Quantum Dots for Luminescent Solar Concentrators. *Sol. RRL* **2020**, *4*, 2000195.
(7) Hill, S. K. E.; Connell, R.; Peterson, C.; Hollinger, J.; Hillmyer, M. A.; Kortshagen, U.; Ferry, V. E. Silicon Quantum Dot−Poly(Methyl Methacrylate) Nanocomposites with Reduced Light Scattering for Luminescent Solar Concentrators. *ACS Photonics* **2019**, *6*, 170−180.
(8) Hill, S. K. E.; Connell, R.; Held, J.; Peterson, C.; Francis, L.; Hillmyer, M. A.; Ferry, V. E.; Kortshagen, U. Poly(Methyl Methacrylate) Films with High Concentrations of Silicon Quantum Dots for Visibly Transparent Luminescent Solar Concentrators. *ACS Appl. Mater. Interfaces* **2020**, *12*, 4572−4578.
(9) Keil, J.; Liu, Y.; Kortshagen, U.; Ferry, V. E. Bilayer Luminescent Solar Concentrators with Enhanced Absorption and Efficiency for Agrivoltaic Applications. *ACS Appl. Energy Mater.* **2021**, *4*, 14102−14110.
(10) Han, S.; Wen, J.; Cheng, Z.; Chen, G.; Jin, S.; Shou, C.; Shou, C.; Kuo, H.-C.; Tu, C.-C. Luminescence-Guided and Visibly Transparent Solar Concentrators Based on Silicon Quantum Dots. *Opt. Express* **2022**, *30*, 26896−26911.
(11) Huang, J.; Zhou, J.; Jungstedt, E.; Samanta, A.; Linnros, J.; Berglund, L. A.; Sychugov, I. Large-Area Transparent "Quantum Dot Glass" for Building-Integrated Photovoltaics. *ACS Photonics* **2022**, *9*, 2499−2509.
(12) Marinins, A.; Zandi Shafagh, R.; van der Wijngaart, W.; Haraldsson, T.; Linnros, J.; Veinot, J. G. C.; Popov, S.; Sychugov, I. Light-Converting Polymer/Si Nanocrystal Composites with Stable 60−70% Quantum Efficiency and Their Glass Laminates. *ACS Appl. Mater. Interfaces* **2017**, *9*, 30267−30272.
(13) Henderson, E. J.; Shuhendler, A. J.; Prasad, P.; Baumann, V.; Maier-Flaig, F.; Faulkner, D. O.; Lemmer, U.; Wu, X. Y.; Ozin, G. A. Colloidally Stable Silicon Nanocrystals with Near-Infrared Photoluminescence for Biological Fluorescence Imaging. *Small* **2011**, *7*, 2507−2516.
(14) Li, Z.; Mahajan, A.; Andaraarachchi, H. P.; Lee, Y.; Kortshagen, U. R. Water-Soluble Luminescent Silicon Nanocrystals by Plasma-Induced Acrylic Acid Grafting and PEGylation. *ACS Appl. Bio Mater.* **2021**, *5*, 105−112.
(15) Erogbogbo, F.; Yong, K.-T.; Roy, I.; Xu, G.; Prasad, P. N.; Swihart, M. T. Biocompatible Luminescent Silicon Quantum Dots for Imaging of Cancer Cells. *ACS Nano* **2008**, *2*, 873−878.
(16) Meier, C.; Gondorf, A.; Lüttjohann, S.; Lorke, A.; Wiggers, H. Silicon Nanoparticles: Absorption, Emission, and the Nature of the Electronic Bandgap. *J. Appl. Phys.* **2007**, *101*, 103112.
(17) Pi, X. D.; Liptak, R. W.; Deneen Nowak, J.; Wells, N. P.; Carter, C. B.; Campbell, S. A.; Kortshagen, U. Air-Stable Full-Visible-Spectrum Emission from Silicon Nanocrystals Synthesized by an All-Gas-Phase Plasma Approach. *Nanotechnology* **2008**, *19*, 245603.
(18) Miller, J. B.; Van Sickle, A. R.; Anthony, R. J.; Kroll, D. M.; Kortshagen, U. R.; Hobbie, E. K. Ensemble Brightening and Enhanced Quantum Yield in Size-Purified Silicon Nanocrystals. *ACS Nano* **2012**, *6*, 7389−7396.
(19) Canham, L. T. Silicon Quantum Wire Array Fabrication by Electrochemical and Chemical Dissolution of Wafers. *Appl. Phys. Lett.* **1990**, *57*, 1046−1048.
(20) Zhou, J.; Huang, J.; Chen, H.; Samanta, A.; Linnros, J.; Yang, Z.; Sychugov, I. Low-Cost Synthesis of Silicon Quantum Dots with Near-Unity Internal Quantum Efficiency. *J. Phys. Chem. Lett.* **2021**, *12*, 8909−8916.
(21) Yu, Y.; Fan, G.; Fermi, A.; Mazzaro, R.; Morandi, V.; Ceroni, P.; Smilgies, D.-M.; Korgel, B. A. Size-Dependent Photoluminescence Efficiency of Silicon Nanocrystal Quantum Dots. *J. Phys. Chem. C* **2017**, *121*, 23240−23248.
(22) Hessel, C. M.; Henderson, E. J.; Veinot, J. G. C. Hydrogen Silsesquioxane: A Molecular Precursor for Nanocrystalline Si−SiO_2 Composites and Freestanding Hydride-Surface-Terminated Silicon Nanoparticles. *Chem. Mater.* **2006**, *18*, 6139−6146.
(23) Takagi, H.; Ogawa, H.; Yamazaki, Y.; Ishizaki, A.; Nakagiri, T. Quantum Size Effects on Photoluminescence in Ultrafine Si Particles. *Appl. Phys. Lett.* **1990**, *56*, 2379−2380.
(24) Mangolini, L.; Thimsen, E.; Kortshagen, U. High-Yield Plasma Synthesis of Luminescent Silicon Nanocrystals. *Nano Lett.* **2005**, *5*, 655−659.
(25) Kramer, N. J.; Anthony, R. J.; Mamunuru, M.; Aydil, E. S.; Kortshagen, U. R. Plasma-Induced Crystallization of Silicon Nanoparticles. *J. Phys. D: Appl. Phys.* **2014**, *47*, 075202.
(26) Gresback, R.; Nozaki, T.; Okazaki, K. Synthesis and Oxidation of Luminescent Silicon Nanocrystals from Silicon Tetrachloride by Very High Frequency Nonthermal Plasma. *Nanotechnology* **2011**, *22*, 305605.
(27) Milliken, S.; Thiessen, A. N.; Cheong, I. T.; O'Connor, K. M.; Li, Z.; Hooper, R. W.; Robidillo, C. J. T.; Veinot, J. G. C. "Turning the Dials": Controlling Synthesis, Structure, Composition, and Surface Chemistry to Tailor Silicon Nanoparticle Properties. *Nanoscale* **2021**, *13*, 16379−16404.
(28) Kortshagen, U. R.; Sankaran, R. M.; Pereira, R. N.; Girshick, S. L.; Wu, J. J.; Aydil, E. S. Nonthermal Plasma Synthesis of Nanocrystals: Fundamental Principles, Materials, and Applications. *Chem. Rev.* **2016**, *116*, 11061−11127.
(29) Jurbergs, D.; Rogojina, E.; Mangolini, L.; Kortshagen, U. Silicon nanocrystals with ensemble quantum yields exceeding 60%. *Appl. Phys. Lett.* **2006**, *88*, 233116.
(30) Sangghaleh, F.; Sychugov, I.; Yang, Z.; Veinot, J. G. C.; Linnros, J. Near-Unity Internal Quantum Efficiency of Luminescent Silicon Nanocrystals with Ligand Passivation. *ACS Nano* **2015**, *9*, 7097−7104.

https://doi.org/10.1021/acsanm.3c01130
ACS Appl. Nano Mater. 2023, 6, 6444−6453

(31) Dasog, M.; Kehrle, J.; Rieger, B.; Veinot, J. G. C. Silicon Nanocrystals and Silicon-Polymer Hybrids: Synthesis, Surface Engineering, and Applications. *Angew. Chem., Int. Ed.* **2016**, *55*, 2322−2339.
(32) Pietryga, J. M.; Park, Y.-S.; Lim, J.; Fidler, A. F.; Bae, W. K.; Brovelli, S.; Klimov, V. I. Spectroscopic and Device Aspects of Nanocrystal Quantum Dots. *Chem. Rev.* **2016**, *116*, 10513−10622.
(33) Zhu, H.; Song, N.; Lian, T. Controlling Charge Separation and Recombination Rates in CdSe/ZnS Type I Core−Shell Quantum Dots by Shell Thicknesses. *J. Am. Chem. Soc.* **2010**, *132*, 15038−15045.
(34) Anthony, R.; Kortshagen, U. Photoluminescence Quantum Yields of Amorphous and Crystalline Silicon Nanoparticles. *Phys. Rev. B: Condens. Matter Mater. Phys.* **2009**, *80*, 115407.
(35) Botas, A. M. P.; Ferreira, R. A. S.; Pereira, R. N.; Anthony, R. J.; Moura, T.; Rowe, D. J.; Kortshagen, U. High Quantum Yield Dual Emission from Gas-Phase Grown Crystalline Si Nanoparticles. *J. Phys. Chem. C* **2014**, *118*, 10375−10383.
(36) Gelloz, B.; Koshida, N. Highly Enhanced Efficiency and Stability of Photo- and Electro-Luminescence of Nano-Crystalline Porous Silicon by High-Pressure Water Vapor Annealing. *Jpn. J. Appl. Phys.* **2006**, *45*, 3462−3465.
(37) Gelloz, B.; Koshida, N. Mechanism of a Remarkable Enhancement in the Light Emission from Nanocrystalline Porous Silicon Annealed in High-Pressure Water Vapor. *J. Appl. Phys.* **2005**, *98*, 123509.
(38) Gelloz, B.; Koshida, N. Long-Lived Blue Phosphorescence of Oxidized and Annealed Nanocrystalline Silicon. *Appl. Phys. Lett.* **2009**, *94*, 201903.
(39) Gelloz, B.; Mentek, R.; Koshida, N. Specific Blue Light Emission from Nanocrystalline Porous Si Treated by High-Pressure Water Vapor Annealing. *Jpn. J. Appl. Phys.* **2009**, *48*, 04C119.
(40) Koyama, H.; Matsushita, Y.; Koshida, N. Activation of Blue Emission from Oxidized Porous Silicon by Annealing in Water Vapor. *J. Appl. Phys.* **1998**, *83*, 1776−1778.
(41) Gelloz, B.; Koyama, H.; Koshida, N. Polarization Memory of Blue and Red Luminescence from Nanocrystalline Porous Silicon Treated by High-Pressure Water Vapor Annealing. *Thin Solid Films* **2008**, *517*, 376−379.
(42) Jang, Y. R.; Yoo, K.-H. Surface Passivation and Bandgap Widening in Poly-Si Treated by Using High-Pressure Water-Vapor Annealing. *J. Korean Phys. Soc.* **2015**, *67*, 355−359.
(43) Kunii, M. Evaluation of Electrical Characteristics and Trap-State Density in Bottom-Gate Polycrystalline Thin Film Transistors Processed with High-Pressure Water Vapor Annealing. *Jpn. J. Appl. Phys.* **2006**, *45*, 660−665.
(44) Ohdaira, K. Defect Termination of Flash-Lamp-Crystallized Large-Grain Polycrystalline Silicon Films by High-Pressure Water Vapor Annealing. *Jpn. J. Appl. Phys.* **2013**, *52*, 04CR11.
(45) Sameshima, T.; Sakamoto, K.; Tsunoda, Y.; Satoh, M. Improvement in SiO_2 Properties by Heating Treatment in High Pressure H_2O Vapor. *Jpn. J. Appl. Phys.* **1998**, *37*, 1452−1454.
(46) Keiji Sakamoto, K. S.; Toshiyuki Sameshima, T. S. Passivation of SiO_2/Si Interfaces Using High-Pressure-H_2O-Vapor Heating. *Jpn. J. Appl. Phys.* **2000**, *39*, 2492.
(47) Sano, N.; Sekiya, M.; Hara, M.; Kohno, A.; Sameshima, T. Improvement of SiO_2/Si Interface by Low-temperature Annealing in Wet Atmosphere. *Appl. Phys. Lett.* **1995**, *66*, 2107−2109.
(48) Sano, N.; Sekiya, M.; Hara, M.; Kohno, A.; Sameshima, T. High Quality SiO_2/Si Interfaces of Poly-Crystalline Silicon Thin Film Transistors by Annealing in Wet Atmosphere. *IEEE Electron Device Lett.* **1995**, *16*, 157−160.
(49) Salhi, B.; Gelloz, B.; Koshida, N.; Patriarche, G.; Boukherroub, R. Synthesis and Photoluminescence Properties of Silicon Nanowires Treated by High-Pressure Water Vapor Annealing. *Phys. Status Solidi A* **2007**, *204*, 1302−1306.
(50) Gelloz, B.; Juangsa, F. B.; Nozaki, T.; Asaka, K.; Koshida, N.; Jin, L. Si/SiO_2 Core/Shell Luminescent Silicon Nanocrystals and Porous Silicon Powders With High Quantum Yield, Long Lifetime, and Good Stability. *Front. Phys.* **2019**, *7*, 47.
(51) Holman, Z. C.; Kortshagen, U. R. A Flexible Method for Depositing Dense Nanocrystal Thin Films: Impaction of Germanium Nanocrystals. *Nanotechnology* **2010**, *21*, 335302.
(52) Mangolini, L.; Jurbergs, D.; Rogojina, E.; Kortshagen, U. Plasma Synthesis and Liquid-Phase Surface Passivation of Brightly Luminescent Si Nanocrystals. *J. Lumin.* **2006**, *121*, 327−334.
(53) Kubin, R. F.; Fletcher, A. N. Fluorescence Quantum Yields of Some Rhodamine Dyes. *J. Lumin.* **1982**, *27*, 455−462.
(54) Natter, H.; Schmelzer, M.; Löffler, M.-S.; Krill, C. E.; Fitch, A.; Hempelmann, R. Grain-Growth Kinetics of Nanocrystalline Iron Studied In Situ by Synchrotron Real-Time X-Ray Diffraction. *J. Phys. Chem. B* **2000**, *104*, 2467−2476.
(55) Borchert, H.; Shevchenko, E. V.; Robert, A.; Mekis, I.; Kornowski, A.; Grübel, G.; Weller, H. Determination of Nanocrystal Sizes: A Comparison of TEM, SAXS, and XRD Studies of Highly Monodisperse CoPt3 Particles. *Langmuir* **2005**, *21*, 1931−1936.
(56) Anthony, R. J.; Rowe, D. J.; Stein, M.; Yang, J.; Kortshagen, U. Routes to Achieving High Quantum Yield Luminescence from Gas-Phase-Produced Silicon Nanocrystals. *Adv. Funct. Mater.* **2011**, *21*, 4042−4046.
(57) San Andrés, E.; del Prado, A.; Mártil, I.; González-Díaz, G.; Bravo, D.; López, F. J.; Fernández, M.; Bohne, W.; Röhrich, J.; Selle, B.; Sieber, I. Bonding Configuration and Density of Defects of SiO_xH_y Thin Films Deposited by the Electron Cyclotron Resonance Plasma Method. *J. Appl. Phys.* **2003**, *94*, 7462−7469.
(58) Pereira, R. N.; Rowe, D. J.; Anthony, R. J.; Kortshagen, U. Freestanding Silicon Nanocrystals with Extremely Low Defect Content. *Phys. Rev. B: Condens. Matter Mater. Phys.* **2012**, *86*, 085449.
(59) Greben, M.; Khoroshyy, P.; Valenta, J. Spectral Dependencies of the Stretched Exponential Dispersion Factor and Photoluminescence Quantum Yield as a Common Feature of Nanocrystalline Si. *Phys. Status Solidi A* **2020**, *217*, 1900698.
(60) Hunter, K. I.; Andaraarachchi, H. P.; Kortshagen, U. R. Nonthermal Plasma Synthesized Silicon-Silicon Nitride Core−Shell Nanocrystals with Enhanced Photoluminescence. *J. Phys. D: Appl. Phys.* **2021**, *54*, 504005.
(61) Linnros, J.; Lalic, N.; Galeckas, A.; Grivickas, V. Analysis of the Stretched Exponential Photoluminescence Decay from Nanometer-Sized Silicon Crystals in SiO2. *J. Appl. Phys.* **1999**, *86*, 6128−6134.
(62) Weeks, S. L.; Chaukulkar, R. P.; Stradins, P.; Agarwal, S. Photoluminescence Behavior of Plasma Synthesized Si Nanocrystals Oxidized at Low Temperature in Pure O_2 and H_2O. *J. Vac. Sci. Technol., A* **2014**, *32*, 050604.
(63) Shu, Y.; Kortshagen, U. R.; Levine, B. G.; Anthony, R. J. Surface Structure and Silicon Nanocrystal Photoluminescence: The Role of Hypervalent Silyl Groups. *J. Phys. Chem. C* **2015**, *119*, 26683−26691.
(64) Mattei, G.; Valentini, V.; Yakovlev, V. A. An FTIR Study of Porous Silicon Layers Exposed to Humid Air with and without Pyridine Vapors at Room Temperature. *Surf. Sci.* **2002**, *502*−*503*, 58−62.
(65) Popelensky, V. M.; Dorofeev, S. G.; Kononov, N. N.; Bubenov, S. S.; Vinokurov, A. A. Room Temperature Oxidation of Si Nanocrystals at Dry and Wet Air. *J. Nanopart. Res.* **2020**, *22*, 54.
(66) Pereira, R. N.; Rowe, D. J.; Anthony, R. J.; Kortshagen, U. Oxidation of Freestanding Silicon Nanocrystals Probed with Electron Spin Resonance of Interfacial Dangling Bonds. *Phys. Rev. B: Condens. Matter Mater. Phys.* **2011**, *83*, 155327.
(67) Liptak, R. W.; Kortshagen, U.; Campbell, S. A. Surface Chemistry Dependence of Native Oxidation Formation on Silicon Nanocrystals. *J. Appl. Phys.* **2009**, *106*, 064313.
(68) San Andrés, E.; del Prado, A.; Martínez, F. L.; Mártil, I.; Bravo, D.; López, F. J. Rapid Thermal Annealing Effects on the Structural Properties and Density of Defects in SiO_2 and SiN_x:H Films Deposited by Electron Cyclotron Resonance. *J. Appl. Phys.* **2000**, *87*, 1187−1192.

https://doi.org/10.1021/acsanm.3c01130
ACS Appl. Nano Mater. 2023, 6, 6444−6453

(69) Selvan, S. T.; Tan, T. T.; Ying, J. Y. Robust, Non-Cytotoxic, Silica-Coated CdSe Quantum Dots with Efficient Photoluminescence. *Adv. Mater.* **2005**, *17*, 1620−1625.
(70) Li, Z.; Kortshagen, U. R. Aerosol-Phase Synthesis and Processing of Luminescent Silicon Nanocrystals. *Chem. Mater.* **2019**, *31*, 8451−8458.

https://doi.org/10.1021/acsanm.3c01130
ACS Appl. Nano Mater. 2023, 6, 6444−6453